Int. J. Mol. Sci. **2002**, *3*, 858-872

International Journal of
Molecular Sciences
ISSN 1422-0067

www.mdpi.org/ijms/

^{15}N Chemical Shifts in Energetic Materials: CP/MAS and *ab Initio* Studies of Aminonitropyridines, Aminonitropyrimidines, and Their *N*-Oxides

Karen L. Anderson[1,*], Lawrence H. Merwin[1], William S. Wilson[1,†] and Julio C. Facelli[2,*]

[1]Naval Air Warfare Center Weapons Division, China Lake CA 93555-6001, U.S.A.
[2]Center for High Performance Computing, University of Utah, Salt Lake City, UT 84112-0190, U.S.A.
[†]Current Address: Weapons Systems Division, Defence Science & Technology Organisation, Edinburgh SA, 5111, Australia.
*Authors to whom correspondence should be addressed; KLA at: ATK Thiokol Propulsion, P.O. Box 707, M/S 245C, Brigham City, UT 84302, U.S.A., KarenL.Anderson@atk.com; JCF at: 155 S 1452 E Rm 405, Salt Lake City, UT 84112-0190, U.S.A., facelli@chpc.utah.edu.

Received: 22 November 2001 / Accepted: 3 May 2002 / Published: 31 August 2002

Abstract: Solid state ^{15}N NMR chemical shift measurements have been performed on a series of nitro- and amino-substituted nitrogen-containing heterocycles that are of interest as potential new insensitive explosives. Due to low solubilities, many of these compounds are not amenable to study by solution state methods. Theoretical calculations of ^{15}N chemical shift parameters have been performed on the structures of interest and are reported herein. The calculated and experimental values are in good agreement. The use of a model that includes intermolecular effects and allows the proton positions of the nearest neighbors to be optimized leads to the best agreement between calculated and experimental values. The theoretical models accurately predict the effects of nitro and amino substituents on ring-nitrogen chemical shifts, explaining a seeming reversal in trend that is noted in the pyridine and pyridine-1-oxide chemical shifts of the highly substituted compounds.

Keywords: Nitrogen-15 solid state NMR, Nitrogen-15 chemical shielding calculations, Aminonitropyridines, Aminonitropyrimidines, Intermolecular effects.

---

1. Introduction

In general, materials that exhibit good explosive properties tend to be sensitive and unstable, while insensitive materials tend to be somewhat lacking in explosive performance. Therefore, an area of great interest is the development of novel energetic materials that perform well but display a reduced sensitivity to environmental stimuli such as rough handling, shock initiation, and thermal cook-off. The benchmark for insensitivity in energetic materials is 1,3,5-triamino-2,4,6-trinitobenzene (TATB). Due to the presence of alternating nitro and amino groups around the ring, this substance exhibits extensive intermolecular and intramolecular hydrogen bonding, which is held to be responsible for its stability and insensitivity [1-3]. Unfortunately, its oxygen balance and energy content are compromised, and it performs indifferently compared to more sensitive explosive performance benchmarks such as cyclotrimethylenetrinitramine (RDX).

To increase the energy content while maintaining insensitivity, one strategy is to utilize the stability of aromatic heterocyclic compounds, adding further stability through alternating nitro and amino groups and incorporating *N*-oxide functionalities in the ring for improved oxygen balance and additional energy. Using this approach, several highly substituted pyridines, pyrimidines, and their *N*-oxides have been investigated [4-6]. The crystalline structures of some of these compounds have been determined by X-ray diffraction, but it is desirable to characterize these materials by other complementary spectroscopic techniques to enhance the understanding of their crystalline and molecular structures and to provide guidance in using non-diffraction techniques to make inferences on their structures. Of great interest is the characterization by solid state NMR (SSNMR), which can provide valuable structural information when diffraction studies are not feasible due to the lack of good-quality single crystals [7].

The great sensitivity of the ^{15}N SSNMR resonance frequencies to molecular structure and environment has been known for many years. However, due to a low natural abundance, a low gyromagnetic ratio, and long relaxation times, most ^{15}N NMR studies have been performed in the solution state [8,9]. Due to the extremely low solubility of many of the compounds of interest, solution state data are unavailable. Recent advances in ^{15}N SSNMR spectroscopy [10-13] make it possible to use the ^{15}N nucleus to probe molecular structure and environments of nitrogen-containing solids.

Ab initio calculations of ^{15}N chemical shifts have been reported since the 1980s [14,15], but recent advances in computational methods and common access to large-scale powerful computers have made it possible to perform these calculations on a routine basis [16,17]. Combining ab initio calculations of chemical shifts with solid state measurements has become an accepted technique to gather insight into the structure of molecular solids [18], even to the extent of including intermolecular interactions in the calculations [19].

The SSNMR ^{15}N chemical shifts of nitro- and amino-substituted pyridines, pyrimidines, and their *N*-oxides have been measured using CP/MAS methods. Ab initio calculations have been performed on these compounds and are compared to the experimentally determined values. The compounds studied

are as follows: 3,5-dinitro-2,4,6-triaminopyridine (**I**), 3,5-dinitro-2,4,6-triaminopyridine-1-oxide (**II**), 2,6-diamino-3,5-dinitropyridine (**III**), 2,6-diamino-3,5-dinitropyridine-1-oxide (**IV**), 5-nitro-2,4,6-triaminopyrimidine (**V**), 5-nitro-2,4,6-triaminopyrimidine-1-oxide (**VI**), and 5-nitro-2,4,6-triaminopyrimidine-1,3-dioxide (**VII**). The numbering scheme used for these compounds is given in Figure 1.

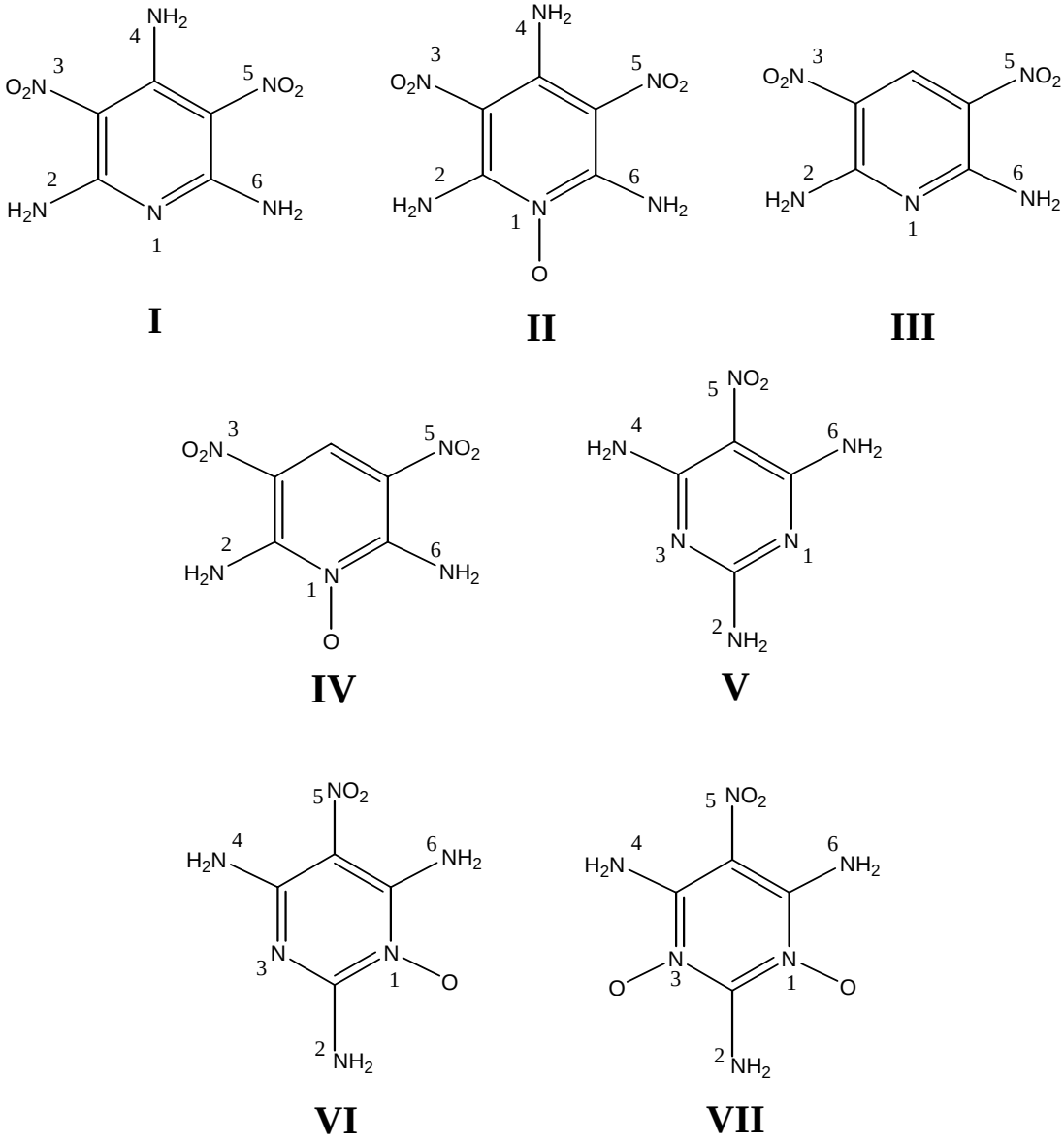

Figure 1. Numbering scheme for the compounds studied.

2. Experimental and Computational Methods

WARNING: Compounds discussed in this article are potentially explosive, and may be subject to accidental initiation by such environmental stimuli as impact, friction, heat, or electrostatic discharge. Therefore, appropriate precautions should be taken in their handling and/or use.

a) Materials

The pyridines were synthesized using methods developed by the authors, which have been reported previously [4]. The pyrimidines were synthesized following the procedure originally described by Delia et al. [20].

b) NMR measurements

Solid state NMR experiments were performed on a Bruker MSL-200 NMR spectrometer operating at a ^{1}H frequency of 200.13 MHz and a ^{15}N frequency of 20.287 MHz. A Bruker 7 mm DB/MAS probe was employed, with typical spinning speeds of 3200 Hz. A standard CP/^{1}H decoupling pulse sequence was used, with typical 90° pulse widths of 5 μs (50 kHz ^{1}H decoupling) and a recycle delay of 10 s. All spectra are referenced to CH_3NO_2 using $^{15}NH_4NO_3$ (room temperature, 1 kHz spinning speed) as a secondary chemical shift reference. $\delta(^{15}NH_4NO_3)$ = -358.4 ppm on this scale.

c) Calculations

All calculations employed the Gauge Invariant Atomic Orbitals (GAIO) [21-23] method with Dunning D95** basis sets [24], which include polarization functions. The Density Functional Theory (DFT) [25,26] calculations use the Becke-Lee-Yang-Parr (BLYP) [27] exchange correlation functional and a coupled perturbative scheme that does not include the magnetic field effects in the exchange correlation functional [28]. The BLYP method was used because it produces results that are significantly better than Hartree Fock (HF) and similar to MP2 at a fraction of the computational cost. Moreover, it has been demonstrated that calculations that use any nonlocal exchange correlation functional produce similar results [28]. The Gaussian 98 suite of programs was used in all the calculations reported [29].

The calculated chemical shieldings were converted to the shift scale by subtracting the shielding values from the absolute shielding value of nitromethane, -135.8 ppm, obtained from the literature [30].

Calculations were done using the following models:

i) Optimized Geometries (OPT): The geometries of all the compounds were optimized using the same method described above to calculate the chemical shifts, i.e., DFT using the BLYP exchange correlation functional and the D95** basis set.

ii) X-ray Geometries (XR): For compounds **I**, **II**, **IV**, **VI**, and **VII,** calculations were performed using the X-ray geometries that were available. The X-ray structures for **I**, **II,** and **IV** have been reported previously [4]. Structures for **VI** and **VII** were available through personal communication [31].

iii) X-ray Geometries with Hydrogen Bonding (HB): Calculations were performed using the X-ray geometries with the effects of the nearest neighboring molecules included to account for intermolecular effects, mainly hydrogen bonding, in the shielding calculations. Calculations using this model were completed for the compounds with known X-ray structures (**I**, **II**, **IV**, **VI,** and **VII)**. To reduce the size of the calculations, only the interacting pieces of the first neighboring molecules were included in the calculations. .pdb files with the geometries used in the calculations are available from the authors (JCF) upon request.

iv) X-ray Geometries with Hydrogen Bonding and Optimized Proton Positions (HB/Hopt): To further improve the model and optimize the contribution due to intermolecular effects, calculations were performed using the geometries in iii, but additionally optimizing the positions of the protons in the model. This procedure was used in view of the well known fact that accurate positions of the protons are necessary to obtain good agreement between the calculated and experimental values of the chemical shifts [32]. The positions of the protons were optimized using the Unified Force Field (UFF) [33,34] as implemented in the Gaussian 98 program.

3. Results and Discussion

Table 1 presents a comparison of the experimental (CP/MAS) ^{15}N chemical shifts and their calculated values using the different models described above. Assignments of the resonances were made based on known trends associated with the functional groups present, symmetry considerations, and relative intensities (in the case of the NH_2 groups). Other techniques, such as slow spinning MAS, were used as necessary to verify the assignments. It should be noted that the NH_2 resonances are broader than the other resonances in the spectrum, due to incomplete ^1H decoupling, but the magnetically nonequivalent groups are still evident in many of the spectra.

As expected, the OPT geometries lead to the symmetrical (magnetically equivalent) chemical shift values that would be expected if no intermolecular interactions were present. This can be seen in both the NH_2 and the NO_2 values for several of the compounds. In the cases where X-ray structures are used as the basis for the calculations, molecular symmetry is lost, and the calculated values generally reproduce the crystallographic nonequivalences seen in the experimental results.

There is a significant improvement in the agreement between experimental and calculated chemical shifts when using the optimized geometries in the calculations. In general, the values calculated with optimized geometries are 20 ppm less shielded than those calculated using experimental geometries, which leads to a significant improvement in the agreement with the experimental values. It is important to note that optimized N-O and N-C distances are ~0.04 Å and 0.03 Å longer, respectively, than the experimental values. This leads to the conclusion that improvements in the results are most likely due to a cancellation of errors in the optimized calculations. Note that increasing the bond length is normally associated with a deshielding effect [35]. This effect is not as conspicuous in the ring nitrogens. The effect is also observed for the NH_2 shifts, but in this case the HB effects are also important. Lack of accurate N-H distances from the X-ray studies makes it difficult to determine if

Table 1. Comparison between experimental chemical shifts and calculated values. All values are referenced to nitromethane as explained in the text.[a]

Structure (Nucleus)[b]	Calculated Values				Exp.[c]
	OPT	XR	HB	HB/Hopt	
I-NO_2 (3)	-21	-43	-45	-47	-13
I-NO_2 (5)	-21	-40	-45	-45	-13
I-N (1)	-165	-173	-179	-180	-194
I-NH_2 (2)	-277	-317	-306	-288	-277 or -274[d]
I-NH_2 (4)	-275	-313	-302	-304	-267
I-NH_2 (6)	-277	-316	-307	-300	-277 or -274[d]
II-NO_2 (3)	-25	-44	-47	-47	-15
II-NO_2 (5)	-25	-44	-47	-48	-15
II-N-O (1)	-160	-166	-170	-173	-186
II-NH_2 (2)	-285	-322	-314	-295	-283 or -279[d]
II-NH_2 (4)	-277	-318	-309	-296	-273
II-NH_2 (6)	-285	-322	-312	-313	-283 or -279[d]
III-NO_2 (3, 5)	-20	-	-	-	-13
III-N (1)	-144	-	-	-	-162
III-NH_2 (2, 6)	-280	-	-	-	-281
IV-NO_2 (3)	-21	-40	-40	-42	-14
IV-NO_2 (5)	-21	-40	-40	-44	-14
IV-N-O (1)	-139	-153	-157	-155	-159
IV-NH_2 (2)	-290	-328	-317	-290	-292
IV-NH_2 (6)	-290	-328	-316	-300	-292
V-NO_2 (5)	-21	-	-	-	-17
V-N (1, 3)	-176	-	-	-	-200, -198[e]
V-NH_2 (4, 6)	-285	-	-	-	-280
V-NH_2 (2)	-295	-	-	-	-290
VI-NO_2 (5)	-26	-51	-53	-53	-19
VI-N-O (1)	-159	-164	-174	-176	-192[f]
VI-N (3)	-193	-196	-202	-205	-213[f]
VI-NH_2 (2)	-300	-340	-310	-298	-271
VI-NH_2 (4)	-294	-334	-322	-310	-289
VI-NH_2 (6)	-286	-327	-322	-307	-289

Table 1. (continued)

Structure (Nucleus)	Calculated Values				Exp.[c]
	OPT	XR	HB	HB/Hopt	
VII-NO_2 (5)	-28	-56	-58	-60	-19
VII-N-O (1)	-166	-171	-182	-185	-198[g]
VII-N-O (3)	-166	-177	-180	-183	-192[g]
VII-NH_2 (2)	-318	-339	-328	-311	-291[h]
VII-NH_2 (4)	-339	-331	-309	-298	-291[h]
VII-NH_2 (6)	-331	-318	-305	-286	-291[h]

[a] Calculated values using the DFT method with the BLYP exchange correlation function and a D95** basis set. The models used for the calculations are described in the methods section.
[b] See Figure 1 for numbering scheme.
[c] Assignments were made based on relative chemical shifts, intensities, and symmetry considerations.
[d] It is not possible to assign these chemical shifts to specific NH_2 groups.
[e] Magnetic nonequivalence of two ring nitrogens was observed in the SSNMR spectrum, but was not reproduced in the calculations because no X-ray structure was available.
[f] Ring-nitrogen assignments were confirmed by comparing the slow-spinning MAS sideband patterns with those of compounds V and VII. The N-O functionality yields a relatively narrow, symmetrical pattern, whereas the non-oxygenated N is broad and asymmetric.
[g] Crystallographically nonequivalent due to the presence of a water of hydration; drying the sample leads to a collapse of these two peaks into a single peak at -192 ppm.
[h] Overlap of crystallographically nonequivalent NH_2 groups due to the presence of a water of hydration; drying the sample leads to a resolution of this resonance into two peaks, one at -289 ppm (**4**, **6**) and one at -296 ppm (**2**).

this is a genuine effect or simply a cancellation of errors as observed in the chemical shifts of the NO_2 groups.

HB effects are only a few ppm for the NO_2 groups (2 - 3 ppm), somewhat larger for the ring nitrogens (~5 ppm) and significant for the NH_2 shifts (~10 ppm). In all cases the inclusion of the intermolecular interactions using the cluster method produces results that are in better agreement with the experimental values.

Table 2 presents a quantitative comparison between the experimental and calculated chemical shifts for the different models using regression analysis. As seen in this table, the correlation is quite good, with the best agreement observed with the use of the optimized geometries. The inclusion of nearest neighbors in the calculations is also seen to improve the agreement. Clearly, the effects of neighboring groups are significant in these crystalline environments, as has been noted in the experimental results via crystallographic nonequivalences.

The principal components of the ^{15}N chemical shift tensors of the compounds of interest, as determined from the DFT calculations using the OPT geometries, are shown in Tables 3 though 5. Table 3 summarizes the NH_2 values, Table 4 the NO_2 values, and Table 5 the ring-nitrogen values. The orientations of the principal values for the NH_2 ^{15}N chemical shift tensors, seen in Table 3, are as would be expected. The most highly shielded component, δ_{33}, is approximately perpendicular to the HNH plane, while δ_{11} bisects the HNH angle and δ_{22} is perpendicular to δ_{11} in the HNH plane.

Table 2. Quantitative comparison between experimental and calculated chemical shifts for the different models considered.

Model	RMS[a]	R^2	Slope	Intercept[a]
OPT[b]	18.9	0.9743	1.01	0.61
XR	26.4	0.9548	1.04	-16.3
HB	20.1	0.9705	0.99	-22.2
HB/Hopt	17.2	0.9758	0.93	-26.8

[a] Values in ppm; the intercept is referenced to nitromethane and includes any systematic errors in the referencing process of both the experimental and calculated values.
[b] Including all the shift values in the linear regression analysis. If only the chemical shifts of the molecules for which the X-ray structures are known are included, the RMS increases to 19.8 ppm, with R^2 = 0.9712, Slope = 1.01 and Intercept = 0.51 ppm.

In Table 3, it can be seen that the δ_{11} principal component of the chemical shift tensor is more sensitive to electronic, structural, and environmental changes in these compounds by a factor of two compared to the other components. The values of δ_{11} in the compounds studied range from -177 ppm to -294 ppm, a difference of 117 ppm. The ranges of the other components and the isotropic values are more modest at 70 ppm for δ_{22}, 56 ppm for δ_{33}, and 64 ppm for the isotropic values.

The orientations of the principal values for the NO_2 ^{15}N chemical shift tensors, shown in Table 4, also agree with what would be expected. The most highly shielded component, δ_{33}, is approximately perpendicular to the ONO plane, while δ_{11} bisects the ONO angle and δ_{22} is perpendicular to δ_{11} in the ONO plane.

The δ_{11} principal components have two different families of values, one at approximately 95 ppm for compounds **III** and **IV** and the other at approximately 75 ppm for the rest of the compounds. In compounds **III** and **IV**, the nitro group has only one NH_2 ortho group, while there are two for the remaining compounds. The δ_{33} principal component is very insensitive in the compounds studied. It varies by less than 5 ppm; a similar behavior is observed for the isotropic values. The δ_{22} principal component has a range similar to that of δ_{11}, but with a less obvious pattern.

The orientations of the principal values for the ring-^{15}N chemical shift tensors, shown in Table 5, also agree with what would be expected. The most highly shielded component, δ_{33}, is approximately perpendicular to the molecular plane, while δ_{11} is in the direction that is tangential to the ring and δ_{22} is perpendicular to δ_{11} in the plane of the molecule. The δ_{11} principal component moves significantly upfield (more shielded) for the N-O ring nitrogens with respect to the pyridinic nitrogens. A similar trend is observed for δ_{22}, while the reverse is observed for δ_{33}.

In comparing the isotropic chemical shifts of the ring nitrogens in compounds **I** and **II**, an interesting trend is noted. While pyridine resonates downfield from pyridine-1-oxide (the isotropic chemical shifts in the solid state are -63 and -98 ppm for pyridine and pyridine-1-oxide, respectively) [12], the reverse is seen to be the case for these highly substituted compounds. This apparent reversal in trend can be explained by considering the substituent effects associated with the

Table 3. Calculated principal components of the $^{15}NH_2$ chemical shift tensors. These values were calculated using the OPT geometries. All values are in ppm referenced to the nitromethane.

Structure (Nucleus)	δ_{11} [a]	δ_{22} [b]	δ_{33} [c]	δ_{iso} [d]
I (2, 6)	-202	-307	-323	-277 (-277, -274)
I (4)	-177	-289	-358	-275 (-267)
II (2, 6)	-211	-302	-341	-285 (-279, -283)
II (4)	-178	-290	-363	-277 (-273)
III (2, 6)	-207	-312	-322	-280 (-281)
IV (2, 6)	-220	-306	-343	-290 (-292)
V (4, 6)	-211	-309	-335	-285 (-280)
V (2)	-247	-284	-354	-295 (-290)
VI (4)	-213	-311	-333	-286 (-289)
VI (6)	-223	-315	-343	-294 (-289)
VI (2)	-243	-320	-338	-300 (-271)
VII (4)	-294	-353	-371	-339 (-291)
VII (6)	-261	-354	-378	-331 (-291)
VII (2)	-248	-334	-371	-318 (-291)

[a] This component is approximately in the direction bisecting the HNH angle.
[b] This component is approximately in the direction perpendicular to δ_{11} in the plane of the amine group defined by HNH.
[c] This component is approximately perpendicular to the HNH plane.
[d] Experimental values in parenthesis.

Table 4. Calculated principal components of the $^{15}NO_2$ chemical shift tensors. These values were calculated using the OPT geometries. All values are in ppm referenced to the nitromethane.

Structure (Nucleus)	δ_{11} [a]	δ_{22} [b]	δ_{33} [c]	δ_{iso} [d]
I (3, 5)	73	36	-171	-21 (-13)
II (3, 5)	74	21	-169	-25 (-15)
III (3, 5)	95	17	-172	-20 (-13)
IV (3, 5)	99	10	-170	-21(-14)
V (5)	73	36	-173	-21 (-17)
VI (5)	74	21	-174	-26 (-19)
VII (5)	77	11	-172	-28 (-19)

[a] This component is approximately in the direction bisecting the ONO angle.
[b] This component is approximately in the direction perpendicular to δ_{11} in the plane of the nitro group defined by ONO.
[c] This component is approximately perpendicular to the ONO plane.
[d] Experimental values in parenthesis.

Table 5. Calculated principal components of the ring-^{15}N chemical shift tensors. These values were calculated using the OPT geometries. All values are in ppm referenced to the nitromethane.

Structure (Nucleus)	δ_{11}[a]	δ_{22}[b]	δ_{33}[c]	δ_{iso}[d]
N				
I (1)	-53	-124	-319	-165 (-194)
III (1)	-13	-103	-315	-144 (-162)
V (1, 3)	-72	-122	-335	-176 (-200, -198)[e]
VI (3)	-92	-140	-346	-193 (-213)
N-O				
II (1)	-90	-142	-246	-160 (-186)
IV (1)	-60	-114	-242	-139 (-159)
VI (1)	-97	-132	-249	-159 (-192)
VII (1)	-99	-147	-251	-177 (-192, -198)

[a] This component is approximately in the direction tangential to the ring.
[b] This component is approximately in the direction perpendicular to δ_{11}, i.e., radial, in the plane of the molecule.
[c] This component is approximately perpendicular to the molecular plane.
[d] Experimental values in parenthesis.
[e] Magnetic nonequivalence of two ring nitrogens was observed in SSNMR spectrum, but was not reproduced in calculations because no X-ray structure was available.

NH_2 and NO_2 groups. Shown in Table 6 is a summary of the calculated effects of ortho, meta, and para substitution of NH_2 and NO_2 groups on the chemical shift of the parent compounds. All values were calculated in the mono-substituted compounds according to the methods described above using fully optimized molecular structures. Experimental values, obtained from solution state measurements, are provided in parenthesis when available.

As seen in Table 6, the agreement between experimental and calculated values of the substituent effects is good. It should be noted that the experimental values may have significant errors due to solvent effects. From this table it is apparent that only the ortho and the para substituent effects are significant, while the meta substituent effect is negligible. Because all of the compounds investigated have NO_2 groups in the meta position, the NO_2 groups have little effect on the ring-nitrogen chemical shifts.

Table 6. Calculated substituent effects in ppm (experimental values, when available, are given in parenthesis)[a]

Position, Group	Pyridine	Pyridine-1-Oxide
***o*-NH_2**	-50 (-53.9)	-34
***m*-NH_2**	0 (-2.7)	0
***p*-NH_2**	-30 (-39.7)	-18
***o*-NO_2**	-23	3
***m*-NO_2**	-4	0
***p*-NO_2**	-24	-10

[a] Solution state values in acetone (see reference 8).

It can also be seen in Table 6 that the effects of ortho- and para-NH_2 substitution are larger for the pyridine than for the pyridine-1-oxide. While the parent pyridine molecule resonates downfield from pyridine-1-oxide, the addition of NH_2 groups shifts both resonances upfield, the pyridine to a greater degree that the pyridine-1-oxide. The net effect is that, as NH_2 substituents are added, the chemical shifts become closer together and eventually cross over one another.

The differential substituent effects for pyridine versus pyridine-1-oxide can be explained by considering the dominant resonance structures of the parent compounds, as illustrated in Figure 2. For the pyridine system (Figure 2(a)), ignoring inductive effects, the π electrons are effectively shared equally throughout the ring. For the pyridine-1-oxide system (Figure 2(b)), due to the interaction of a lone pair of electrons from an oxygen atom with the π electrons in the ring, other resonance structures are possible in which the π electrons are localized. This partial localization of charge forces the substituent effects to be transmitted through at least one formal single bond. Substituents effects are known to be smaller in aliphatic than in aromatic compounds, consistent with the decreased effectiveness observed in pyridine-1-oxide compared to pyridine.

The ring-nitrogen chemical shifts of the compounds studied, calculated using the experimental values of the parent compounds in the solid state and adding theoretically calculated substituent effects, are given in Table 7, along with the experimental values and the values calculated using the OPT structure. Both theoretical methods correlate reasonably well with the experimental values and reproduce the trends discussed previously. However, the values calculated using the quantum mechanical method show a significantly better correlation with the experimental ones (RMS = 5.7 ppm) than do those calculated using empirical methods (RMS = 12.5 ppm). It should be noted that, in both cases, intermolecular interactions have been neglected; therefore, larger discrepancies between the theoretical and the experimental values are expected.

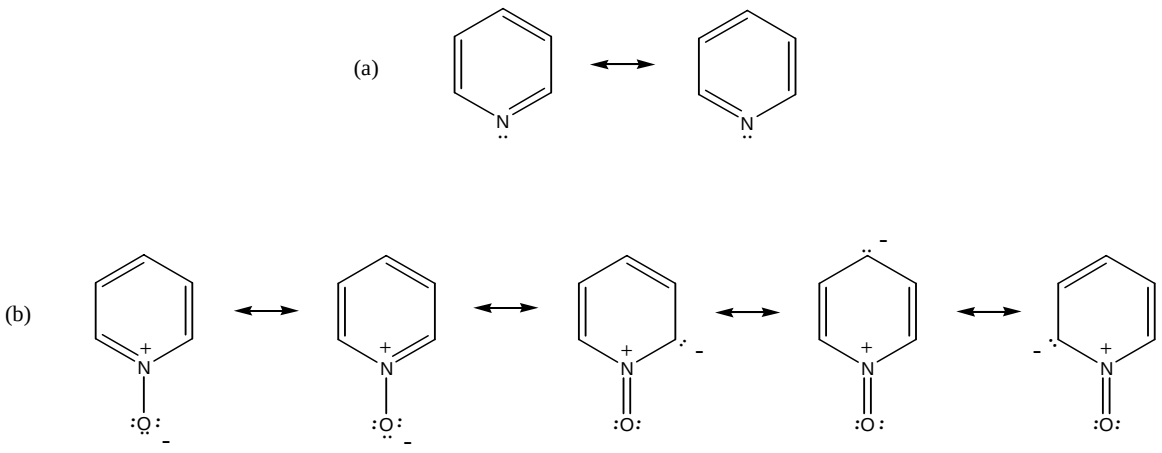

Figure 2. Resonance structures of (a) pyridine and (b) pyridine-1-oxide.

Table 7. Calculated chemical shifts of ring nitrogens using DFT and substituent effect approaches. All values are in ppm referenced to nitromethane.

Structure (Nucleus)	Exp.	Theor.[a]	Subst. Effect[b]
I	-194	-165	-201
II	-186	-160	-184
III	-162	-144	-171
IV	-159	-139	-166
V	-200	-176	-219
	-198		
VI (N)	-213	-193	-214
VI (N-O)	-192	-159	-176
VII	-198	-166	-176
	-192		

[a] Calculated using OPT structures.
[b] Calculated using experimental values of parent compounds (see text) and adding theoretically calculated substituent effects.

4. Conclusions

^{15}N SSNMR chemical shift data have been obtained for a series of highly substituted nitrogen-containing heterocycles. Solution state data of many of these compounds are unavailable due to low solubilities. Theoretical calculations of chemical shifts have been used to aid in the interpretation of the experimental results. The trends observed in the experimental ring-nitrogen values can be explained based on theoretically calculated substituent effects.

From the results obtained, it is clear that the ^{15}N chemical shifts are very sensitive to electronic structure and crystallographic effects. The theoretically calculated results vary significantly depending on the structural model chosen for the calculations. The agreement between theoretically calculated values and experimental results is improved when optimized geometries are included. However, it is not clear if this is a fortuitous cancellation of errors, which appears to be the case for the NO_2 chemical shifts, or a true effect. The lack of accurate experimental positions for the protons makes it more difficult to draw any conclusion for the NH_2 shifts.

The inclusion of hydrogen bonding to neighboring molecules, through the use of the nearest neighbor approximation, makes a significant difference, as great as 10 ppm in the calculated (isotropic) values for the NH_2 chemical shifts. In all cases, inclusion of these effects improves the agreement between experimental and calculated components. In addition, the use of substituent effects to predict chemical shift values leads to values that are in good agreement with experimental results.

Acknowledgments

Computer time for this project was provided by the Center for High Performance Computing at the University of Utah and the Maui High Performance Computing Center, Kihei, Maui, Hawaii. The authors gratefully acknowledge Dr. Richard Gilardi, Naval Research Laboratory, for providing X-ray

data on the pyrimidine heterocycles. KLA is grateful for the support of an American Society for Engineering Education (ASEE) postdoctoral fellowship. LHM and WSW thank the Office of Naval Research, Mechanics Division for financial support.

References

1. Cady, H. H.; Larson, A. C. The Crystal Structure of 1,3,5-triamino-2,4,6-trinitrobenzene. *Acta Crystallogr.* **1965**, *18*, 485-496.
2. Fried, L. E.; Ruggiero, A. J. Energy Transfer Dynamics and Impact Sensitivity. *Matl. Res. Soc. Symp. Proc.* **1993**, *296*, 35-40.
3. Sharma, J.; Beard, B. C. In *Chemistry and Physics of Energetic Materials*; Bulusu, S., Ed.; Kluwer: Dordrech, 1990; p 581.
4. Hollins, R. A.; Merwin, L. H.; Nissan, R. A.; Wilson, W. S.; Gilardi, R. Aminonitropyridines and their *N*-Oxides. *J. Heterocycl. Chem.* **1996**, *33*, 895-904.
5. Altmann, K. L.; Merwin, L. H.; Nissan, R. A.; Wilson, W. S., "Solid State ^{13}C and ^{15}N NMR Investigations of Novel Pyridines, Pyrimidines, and their *N*-Oxides," Poster #263, 37th Rocky Mountain Conference on Analytical Chemistry, Denver, CO, July 23 - 27, 1995.
6. Altmann, K. L.; Merwin, L. H.; Nissan, R. A.; Wilson, W. W., "Solid State NMR Investigations of Novel Pyridines, Pyrimidines, and their *N*-Oxides: Reversed Ring-Nitrogen Shift Assignments," Poster #WP264, 37th Experimental NMR Conference, Asilomar, CA, March 17 - 26, 1996.
7. Facelli, J. C.; Grant, D. M. Determination of Molecular Symmetry in Crystalline Naphthalene Using Solid-State NMR Data. *Nature* **1993**, *365*, 325-327.
8. Witanowski, M.; Stefaniak, L.; Webb, G. A. "Nitrogen NMR Spectroscopy" In *Annu. Rep. NMR Spectrosc.*; Webb, G. A., Ed.; Academic Press: London, 1993; Vol. 25, pp 1-480.
9. Mason, J. "Nitrogen NMR" In *Encyclopedia of Nuclear Magnetic Resonance*; Grant, D. M. and Harris, R. K., Eds.; John Wiley: London, 1996; p 3222.
10. Hu, J. Z.; Zhou, J.; Yang, B.; Li, L.; Qiu, J.; Ye, C.; Pugmire, R. J.; Solum, M. S.; Wind, R.; Grant, D. M. Dynamic Nuclear Polarization of Nitrogen-15. *Solid State NMR* **1997**, *8*, 129-137.
11. Anderson-Altmann, K. L.; Phung, C. G.; Mavromoustakos, S.; Zheng, Z.; Facelli, J. C.; Poulter, C. D.; Grant, D. M. The ^{15}N Chemical Shift Tensors of Uracil Determined from ^{15}N Powder Pattern and ^{15}N-^{13}C Dipolar NMR Spectroscopy. *J. Phys. Chem.* **1995**, *99*, 10454-10458.
12. Solum, M. S.; Altmann, K. L.; Strohmeier, M.; Berges, D. A.; Zhang, Y.; Facelli, J. C.; Pugmire, R. J.; Grant, D. M. ^{15}N Chemical Shift Principal Values in Nitrogen Heterocycles. *J. Am. Chem. Soc*. **1997**, *119*, 9804-9809.
13. Facelli, J. C.; Pugmire, R. J.; Grant, D. M. Effects of Hydrogen Bonding in the Calculation of ^{15}N Chemical Shift Tensors: Benzamide. *J. Am. Chem. Soc*. **1996**, *118*, 5488-5489.
14. Giessner-Prette, C. J. Ab-Initio Quantum Mechanical Calculations of NMR Chemical Shifts in Nucleic Acid Constituents. I. The Watson-Crick Base Pair. *J. Biomol. Struct. Dynamics* **1984**, *2*, 233-248.
15. Schindler, M. Magnetic Properties in Terms of Localized Quantities. 9. The DNA Bases, and the Protonation of Adenine. *J. Am. Chem. Soc*. **1988**, *110*, 6623-6630.

16. Facelli, J. C. “Shielding Tensor Calculations” In *Encyclopedia of Nuclear Magnetic Resonance*; Grant, D. M. and Harris, R. K., Eds.; John Wiley: London, 1996; pp 4327-4334.
17. Facelli, J. C. In *Modeling NMR Chemical Shifts: Gaining Insights into Structure and Environment*; Facelli, J. C. and de Dios, A. C., Eds.; American Chemical Society Symposium Series, Oxford University Press: London, 1999; No. 732.
18. de Dios, A. C.; Oldfield, E. Recent Progress in Understanding Chemical Shifts. *Solid State NMR* **1996**, *6*, 101-125.
19. Ferraro, M. B.; Repetto, V.; Facelli, J. C. Modeling NMR Chemical Shifts: A Comparison of Charge Models for Solid State Effects on ^{15}N Chemical Shift Tensors. *Solid State NMR* **1998**, *10*, 185-189.
20. Delia, T. J.; Portlock, D. E.; Venton, D. L. Pyrimidine *N*-Oxides. Oxidation of 5-nitroso-2,4,6-triaminopyrimidine. *J. Heterocycl. Chem.* **1968**, *5*, 449-451.
21. London, F. Quantum Theory of Interatomic Currents in Aromatic Compounds. *J. Phys. Radium* **1937**, *8*, 397-409.
22. Ditchfield, R. Self-Consistent Perturbation Theory of Diamagnetism. I. A Gage-Invariant LCAO (Linear Combination of Atomic Orbitals) Method for NMR Chemical Shifts. *Mol. Phys*. **1974**, *27*, 789-807.
23. Wolinski, K.; Hinton, J. F.; Pulay, P. Efficient Implementation of the Gauge-Independent Atomic Orbital Method for NMR Chemical Shift Calculations. *J. Am. Chem. Soc.* **1990**, *112*, 8251-8260.
24. Dunning, T. H.; Hay, P. J. In *Modern Theoretical Chemistry*; Schaefer III, H. F., Ed.; Plenum: New York, 1976; p 1.
25. Hohenberg, P.; Khon, W. Inhomogeneous Electron Gas. *Phys. Rev.* **1964**, *136*, B864-B871.
26. Khon, W.; Sham, L. J. Self-Consistent Equations Including Exchange and Correlation Effects. *Phys. Rev*. **1965**, *140*, A1133-A1138.
27. (a) Becke, A. D. Density-Functional Exchange-Energy Approximation with Correct Asymptotic Behavior. *Phys. Rev. A* **1988**, *38*, 3098-3100. (b) Lee, C.; Yang, W.; Parr, R. G. Development of the Colle-Salvetti Correlation-Energy Formula into a Functional of the Electron Density. *Phys. Rev. B* **1988**, *37*, 785-789.
28. Cheeseman, J. R.; Trucks, G. W.; Keith, T. A.; Frisch, M. J. A Comparison of Models for Calculating Nuclear Magnetic Resonance Shielding Tensors. *J. Chem. Phys*. **1996**, *104*, 5497-5509.
29. Frisch, M. J.; Trucks, G. W.; Schlegel, H. B.; Scuseria, G. E.; Robb, M. A.; Cheeseman, J. R.; Zakrzewski, V. G.; Montgomery, J. A., Jr.; Stratmann, R. E.; Burant, J. C.; Dapprich, S.; Millam, J. M.; Daniels, A. D.; Kudin, K. N.; Strain, M. C.; Farkas, O.; Tomasi, J.; Barone, V.; Cossi, M.; Cammi, R.; Mennucci, B.; Pomelli, C.; Adamo, C.; Clifford, S.; Ochterski, J.; Petersson, G. A.; Ayala, P. Y.; Cui, Q.; Morokuma, K.; Malick, D. K.; Rabuck, A. D.; Raghavachari, K.; Foresman, J. B.; Cioslowski, J.; Ortiz, J. V.; Baboul, A. G.; Stefanov, B. B.; Liu, G.; Liashenko, A.; Piskorz, P.; Komaromi, I.; Gomperts, R.; Martin, R. L.; Fox, D. J.; Keith, T.; Al-Laham, M. A.; C. Peng, Y.; Nanayakkara, A.; Gonzalez, C.; Challacombe, M.; Gill, P. M. W.; Johnson, B.; Chen, W.; Wong, M. W.; Andres, J. L.; Gonzalez, C.; Head-Gordon, M.; Replogle, E. S.; Pople, J. A. Gaussian 98, Rev. A.7; Gaussian, Inc.: Pittsburgh, 1998.

30. Jameson, J. C.; Mason, J. In *Multinuclear NMR*; Mason, J., Ed.; Plenum: New York, 1987; p 56.
31. Gilardi, R., Naval Research Laboratory, unpublished results.
32. Grant, D. M.; Liu, F.; Iuliucci, R. J.; Phung, C. G; Facelli, J. C.; Alderman, D. W. Relationship of ^{13}C Chemical Shift Tensors to Diffraction Structures. *Acta Crystallogr., Sect. B* **1995**, *51*, 540-546.
33. Rappé, A. K.; Casewit, C. J.; Colwell, K. S.; Goddard III, W. A.; Skiff, W. M. UFF, a Full Periodic Table Force Field for Molecular Mechanics and Molecular Dynamics Simulations. *J. Am. Chem. Soc.* **1992**, *114*, 10024-10035.
34. Rappé A. K.; Goddard III, W. A. Charge Equilibration for Molecular Dynamics Simulations. *J. Phys. Chem.* **1991,** *95*, 3358-3363.
35. Jameson, C. J.; Osten, H. J. "Theoretical Aspects of Isotope Effects on Nuclear Shielding" In *Annu. Rep. NMR Spectrosc*.; Webb, G. A., Ed.; Academic Press: London, 1986; Vol. 17, pp 1-78.